

1 **Shallow Geophysical Techniques to Investigate the Groundwater Table**
2 **at the Giza Pyramids Area, Giza, Egypt**

3
4 *S. M. Sharafeldin^{1,3}, K. S. Essa¹, M. A. S. Youssef², H. Karli³, and Z. E. Diab¹, N. Sayil³*

5 ¹*Geophysics Dept, Faculty of Science, Cairo University*

6 ²*Nuclear Material Authority, P.O. Box 530, Maadi, Cairo*

7 ³*Geophysical Engineering Dept, KTU, Turkey*

8 *shokryam@yahoo.com*

9 **ABSTRACT**

10 The near surface groundwater aquifer that threatened the Great Giza Pyramids of Egypt,
11 investigated using integrated geophysical surveys. Ten Electrical Resistivity Imaging, 26
12 Shallow Seismic Refraction and 19 Ground Penetrating Radar surveys conducted in the Giza
13 Pyramids Plateau. Acquired data of each method subjected to state- of- the art processing and
14 modeling techniques. A three-layer model depicts the subsurface layers and better delineates the
15 groundwater aquifer and water table elevation. The aquifer layer resistivity ranges between 40-
16 80 Ω m and seismic velocity of 1500-1800 m/s. The average water table elevation is about +15
17 meters which is safe for Sphinx Statue, and still subjected to potential hazards from Nazlet
18 Elsamman Suburban. Shallower water table in Valley Temple and Tomb of Queen Khentkawes
19 detected to be between 14.5-15m represent a sever hazards. Perched ground water table detected
20 in elevated topography to the west and southwest might be due to runoff and capillary seepage.

21
22 *Keywords: Groundwater, Electrical Resistivity, Seismic refraction, GPR.*

23
24 **I. INDRDUCTION**

25 In recent years, the 4500 years old Giza Great Pyramids (GGP) of Egypt; Cheops
26 (Khufu), Chephren (Khafre), Menkaure and Sphinx statue; threatened from the rising
27 groundwater table resulted from the water leakage of the suburban, irrigation canals and mass
28 urbanization surrounding the GGP. This problem promoted the need to use non-destructive near
29 surface geophysical techniques integrated with available borehole hydrogeological data to
30 investigate and characterize the groundwater occurrences in the GGP. The GGP located in the
31 southwestern part of the Greater Cairo Region (Fig. 1). Geologically, the Giza Pyramids Plateau
32 composes mainly of white limestone, cream and yellow argillaceous limestone and dark grey
33 dolomitic limestone of Middle-Upper Eocene age. The plateau rocks are commonly interbedded
34 with thin marl layers in their upper part, which dips with about 5-10° to the SE direction. Steep
35 escarpments border the plateau to the north and east directions as shown in Fig. 2 (Yehia, 1985;
36 Mahmoud and Hamdan, 2002). Two regional groundwater aquifers underlie the sphinx (Fig. 3),
37 the Quaternary aquifer of the Nile alluvium, consists of graded sand and gravel with

38 intercalations of clay lenses at different depths exhibit water table at depth ranges between 1.5 to
39 4 meters bgs. The second aquifer is fissured carbonate aquifer that covers the area below the
40 Pyramids Plateau and the Sphinx, where water table ranges in depth of 4 – 7 m bgs. The recharge
41 of the aquifer below Sphinx area occurred mainly through water system leakage, Irrigation and
42 massive urbanization (AECOM, 2010; and El-Arabi et al., 2013).

43 Many geophysical studies carried out in the GGP mostly for archaeological exploration
44 and investigations (e.g., Dobecki, T. L., 2005; Abbas et al., 2009 and 2012). Geophysical studies
45 have an effective contribution in characterizing groundwater aquifers especially geoelectrical
46 resistivity, seismic refraction and ground penetrating radar techniques. Sharafeldin et al. (2017)
47 studied the occurrence of the ground water table in GGP using combined VES, ERI and GPR to
48 investigate the groundwater table in the area. The present work implemented an integration of
49 Electrical Resistivity Imaging (ERI), Shallow Seismic Refraction (SSR), and Ground Penetrating
50 Radar (GPR) techniques to depict the groundwater table and characterize the aquifer in the Giza
51 Pyramids area. Figure-4 represents the locations of different surveys conducted in the GGP.

52 **II. Method**

53 **II.1 Electrical Resistivity Imaging (ERI) Surveys**

54 Two-dimensional electrical resistivity imaging (tomography) surveys are usually carried
55 out, using a multi-electrode system, 24 or more, connected to a multi-core cable (Griffiths and
56 King, 1965). Syscal-Pro resistivity meter, IRIS Instruments, France, was deployed at the site of
57 the GGP using 24 multi-electrode dipole-dipole array configuration with 5m electrode spacing.
58 The length of spread is 115m for each profile and attains 23.5 m maximum depth of
59 investigation. Ten ERI profiles were performed to characterize the subsurface layers resistivities
60 to delineate the groundwater aquifer (Fig. 4). The topographic elevation of each electrode is
61 considered along ERI profile and fed to the Res2Dinv program. The acquired ERT data were
62 processed using, Prosys II software of IRIS Instruments, to filter and exterminate bad and noisy
63 data acquired in the field and produced the pseudo resistivity sections. The RES2DINV software
64 implemented to invert collected data along conducted ERT profiles (Loke, and Barker, 1996;
65 Loke, 2012). This software works based upon automatically subdividing the subsurface of
66 desired profile into several rectangular prisms and then applies an iterative least-squares
67 inversion algorithm for solving a non-linear set of equations to determine apparent resistivity
68 values of the assumed prisms while decreasing the misfit values between the predicted and the
69 measured data. Samples of interpreted data are shown in Figures 5 to 10.

70

71

72 II.2 Shallow Seismic Refraction (SSR)

73 Seismic refraction is widely used in determining the velocity and depth of weathering
74 layer, static corrections for the deeper reflection data. It is also employed in civil engineering for
75 the bedrock investigations and large scale building construction. It is also used in groundwater
76 investigations, detection of fracture zones in hard rocks, examining stratigraphy and
77 sedimentology, detecting geologic faults, evaluating karst conditions and for hazardous waste
78 disposal delineation (Steeple, 2005; Stipe, 2015). A refraction technique is widely developed
79 for characterizing the groundwater table (Grelle and Guadagno, 2009). Particularly, the
80 unsaturated soil followed by saturated soil can be separated by a refracting interface or surface
81 (Haeni, 1988). The seismic velocity values for the depth estimation of the groundwater can be
82 used as an indicator for water saturation. The values of VP velocity are not uniquely correlated to
83 the aquifer layer, but many authors related the P-wave velocities around 1500 m/s to represent a
84 saturated layer (Grelle and Guadagno, 2009). The tomographic studies view that the water table
85 corresponds to a P-wave velocity values of 1100 to 1200 m/s (Azaria et al., 2003; Zelt et al.,
86 2006).

87 Twenty-six SSR profiles were acquired at GGP (Fig. 4). 24 geophones-channels OYO
88 McSEIS-SX seismograph was deployed in the GGP site to collect the seismic refraction data
89 with geophone spacing is 5m. 10Kg sledge hammer and an iron plate are used to generate
90 seismic P-wave. Five shots per spread were gathered, two off-set forward and reverse, and a split
91 spread shot. The spread length covers 115m. Due to the historical and touristic nature of the site,
92 a considerable amount of noise is imposing to the recorded data. These noises were minimized as
93 possible by using the internal frequency domain filter and stacking of several shots during data
94 acquisition. The first arrival times were picked using SeisImager software version 4.2 of OYO.
95 The time-distance curve constructed and initial model for seismic tomography inversion of
96 velocity and depth of the layered earth. Tomographic inversion; generate initial model from the
97 velocity model obtained by the time-term inversion, then applying the inversion, which
98 iteratively traces rays through the model with the goal of minimizing the RMS error between the
99 observed and calculated travel-times curves (Schuster, 1998). SeisImager utilize a least squares
100 approach for the inversion step (Zhang and Toksoz, 1998; Sheehan et al., 2005; Valenta, 2007).
101 A three layers model assumed to represent the subsurface succession with the inverted velocities
102 and thicknesses. The top most layer exhibits a velocity range of 400-900 m/s, and thickness of 2
103 and 5 meters, is correlated with loose dry sand, fill and debris. The second layer shows a velocity
104 range between 1200 and 2400 m/s with 10 to 20 m thick. This layer is correlated with wet and
105 saturated sand and fractured limestone. The third layer shows a higher domain of velocity, where

106 it ranges between 2800 and 3800 m/s, which can be correlated to marly limestone and limestone.
107 Samples of interpreted data are shown in Figures 5 to 10.

108 **II.3 Ground Penetrating Radar (GPR) techniques**

109 GPR is a non-invasive geophysical technique and effective tool to visualize the near
110 surface structure of the shallow subsurface and widely used to solve the environmental and
111 engineering problems (Jol and Bristow, 2003; Comas et al., 2004; Neal, 2004). GPR is a site-
112 specific technique that imposed a vital limitation of the quality and resolution of the acquired
113 data (Daniels, 2004). The GPR surveys were carried out using 100 MHz shielded antenna of
114 MALA ProEx GPR. 19 GPR profiles were performed along selected locations in the study area
115 (Figure 4). The lengths of GPR profiles range from 40 to 200 m according to the space
116 availability with a total of total GPR survey of about 2.5 kilometer. Wheel calibration was made
117 near the Great Sphinx along 30 m in distance, the velocity used in calibration is 100 m/ μ s using
118 unshielded Puls Echo GPR. Harari (1996) showed that the groundwater table can be detected
119 easily with a discerning selection of the antenna frequency and he observed that the lower
120 frequency antenna (e.g.100 MHz) was more effective for locating the groundwater table depth.
121 Several basic processing techniques can be applied to GPR raw data starting from DC-shift to
122 migration (Annan, 2005; Benedetto et al., 2017). All GPR sections along 19 profiles were
123 processed to delineate subsurface layering and ground water elevation in the study area. To
124 acquire better results, appropriate processing sequence of GPR data was applied to facilitate
125 interpretation of radargram sections using REFLEXWIN V. 6.0.9 software. Time-zero correction
126 filter first applied to all raw GPR data. Dewow Filter was applied to remove direct current and
127 very low frequency components. A band-pass filter used to improve the visual quality of the
128 GPR data. Gain recovery applied to enhance the appearance of later arrivals because the effect of
129 signal attenuation and geometrical spreading losses (Cassidy, 2009). Running average filters was
130 the last filter applied. Samples of interpreted data are shown in Figures 5 to 10.

131 **III. Results and discussion**

132 The integrated interpretation of the SSR, ERI and GPR surveys supported a three layers
133 model assumed to represent the subsurface succession with the inverted velocities, resistivities
134 and thicknesses. The top most layer exhibits a velocity range of 400-900 m/s and a resistivity
135 values varies between 10's to 100's Ohm.m and is correlated with heterogenous loose dry fill
136 and debris of thickness ranges between 2 and 5 meters. The second layer shows a velocity range
137 between 1200 and 2400 m/s and a resistivity values varies between 40 to 80 Ohm.m, this layer is
138 correlated with wet and saturated sand and fractured limestone and the thickness varies between
139 10 to 15 meters. The third layer shows a high velocity ranges between 2800 to 3800 m/s and a

140 resistivity values varies by changing the topographic elevation and marl intercalation in the
141 limestone layer. GPR data delineated the subsurface succession and accurate detection of the
142 water table in area near Sphinx, Valley Temple, Mastaba and Tombs. The ground water table
143 detected ranges between 14-16 meters in these locations. As the ground relief increases toward
144 the Mankaura Pyramids the water table is deeper and a perched water table detected in elevations
145 between 22 to 45 meters.

146 Groundwater rise was detected in some locations of archaeological importance, these
147 locations are Nazlet El-samman Village, Sphinx, Sphinx Temple, Valley Temple of Khafre,
148 Central Field of Mastaba and Khafre Cause Way.

149 **a- Nazlet El-samman Village** is a suburban area located outside the core of the
150 archeological site. The integration of different geophysical surveys conducted in this part,
151 SSR-3 & 4, and GPR-2, revealed that the groundwater elevation at this part is about 16 m
152 asl. The tomogram of SSR-3 & 4 show velocity of 1600-1800 m/s at elevation of 16 m
153 asl. This elevation is fairly coinciding with the results of GPR-2 where a ground water
154 level interpreted to be at 16 m elevation. The aquifer in this part is belonging to the Nile
155 Alluvium Aquifer. The interpreted water table elevation between 16 and 17 m asl. This
156 higher water table might affect the water table level below Sphinx area (Fig. 5).

157 **b- Sphinx, Sphinx Temple, Valley Temple of Khafre, Central Field of Mastaba and**
158 **Khafre Cause Way**, this is the most important part of the study where the water appear
159 on the surface at the Valley temple and surrounding area of the Sphinx. The locations of
160 the surveys were chosen according to the limited space approved by the Pyramid
161 Archaeological Authority. The locations of the conducted data are shown in (Fig.4).
162 Survey shows good matching between the different techniques, where the correlation
163 between different surveys results, revealed that groundwater elevation between 14-15 m
164 asl. This level is lower than the suburban area of Nazlet El-samman, which might indicate
165 a recharge of the aquifer below Sphinx and increase capillary water rise.

166 **Sphinx and Sphinx Temple**, GPR-9, SSR-13 and ERI-1 conducted in front of Sphinx and
167 Sphinx Temple. The integration of these surveys in front of Sphinx Temple, the
168 groundwater elevation is about 14.5-15.5 m asl, as shown in Figure 6.

169 **Valley Temple of Khafre and central field of Mastaba**, GPR profiles 3, 4, 5, 10 and 11;
170 SSR profiles 5, 6, 7, 8 and 14; and ERI 2. The integration of this surveys in front of
171 Valley Temple of Khafre and central field of Mastaba, the groundwater elevation is about
172 14-15 m asl as shown in Figure 7.

173 *Tomb of queen Khentkawes*, GPR-11; SSR-15; and ERI-3 conducted near the Tomb.
174 Figure 7 shows the surveys conduct near the site. The integration of this surveys in front
175 of Valley Tomb of queen Khentkawes, the groundwater elevation is about 14.5-15 m asl.

176 *Valley Temple of Menkaure*, GPR-12; SSR-16; and ERI-4 conducted near the Temple.
177 The integration of these surveys in front of Valley Temple of Menkaure, the groundwater
178 elevation is about 16.5-17 m asl. GPR profiles might detect the perched ground water
179 table at shallower depth from ground level (Fig. 8).

180 *Cause way to Menkaure Pyramid*, show high resistivity value near the surface, and water
181 table located at elevation ranges from 22 to 24 m asl. *Menkaure Queens Pyramids and*
182 *Menkaure Quarry*, where the surveys in this part conducted at higher topographic relief,
183 the correlation of the different techniques revealed that the water table might be
184 interpreted at elevations 45-58 m asl. This might detect the perched ground water table at
185 shallower depth from ground level (Figs. 9 and 10).

186 Figure 11 represents a cross-section, using the ERT and GPR data, to illustrate the difference
187 of groundwater table elevation between the Great Sphinx to the small pyramids of Menkaure that
188 indicates the increase of groundwater elevation from west to east. As the average water table
189 elevation to be about 15 m bsl, the water table to the west can be considered as perched water
190 table to due leakage, surface runoff and capillary and fracture seepage. Figure 12 represents the
191 compiled groundwater table elevation contour map from the geophysical surveys, overlay the
192 groundwater table levels measured from some of the Piezometers installed by Cairo University
193 (AECOM 2010). The present geophysical surveys proved that, the pumping system installed by
194 AECOM 2010 lowering the groundwater levels in some piezometer and a need of more pumping
195 to compensate the recharge of the water leakage resulted from surrounding area of Sphinx.
196 Figure 13 shows a 3D representation of the groundwater system in Great Giza Pyramids Plateau
197 and surrounding area.

198
199
200
201
202
203
204
205
206

207
208
209
210
211
212
213
214
215
216
217
218
219
220
221
222
223
224
225
226
227
228
229
230
231
232
233
234
235
236
237
238
239
240
241

V. Conclusions

The integrated interpretation of ERT, SSR and GPR surveys conducted in Great Giza Pyramids site successfully investigate the groundwater aquifer and water table depth in Great Giza Pyramid and assist the hazards mitigation in a great historical heritage. An interpreted model consists of three layers assumed to depict the subsurface layers and better delineation of the aquifer layer associated with resistivity range of 40-80 Ω m and seismic velocity of 1500-1800 m/s. The average water table depth is about 15m asl, which is safe for the Sphinx status where the foot at elevation of 20 m asl. The water table elevation increases in Nazlet Elsamman Village to 16m and causes leakage towards the Sphinx and Valley Temple which considered a serious hazard to the site. Tomb of Queen Khentkawes threatened by water leakage resulted from vegetation in old cemetery and nearby football field. A parched groundwater table might exist in elevated area toward west and southwest. A great care should be taken to the effect of massive urbanization to the west of the Great Giza Pyramids which might affect the groundwater model of the area. The dewatering system should be accomplished to avoid such hazards.

Acknowledgements

Authors would like to thank Prof. Jothiram Vivekanandan, Chief-Executive Editor, Prof. Andrea Benedetto, the Associate Editor and the reviewer for their constructive comments for improving our manuscript.

242 **References**

- 243 Abbas, A. M., Atya, M., EL-Emam, A., Ghazala, H., Shabaan, F., Odah, H., El-Kheder, I., and
244 Lethy, A.: Integrated Geophysical Studies to Image the Remains of Amenemeht- II Pyramid's
245 Complex in Dahshour Necropolis, Giza, Egypt. NRIAG, 2009.
246 <https://www.researchgate.net/publication/234180809>.
- 247
- 248 Abbas, A. M., El-sayed, E. A., Shaaban, F. A., and Abdel-Hafez, T.: Uncovering the Pyramids-
249 Giza Plateau in a Search for Archaeological Relics by Utilizing Ground Penetrating Radar.
250 *Journal of American Science*, 8(2), 1-16, 2012.
- 251
- 252 AECOM, ECG, and EDG: Pyramids Plateau Groundwater Lowering Activity. Groundwater
253 Modeling and Alternatives Evaluation. USAID Contract No EDH-I-00-08-00024-00-Order
254 No.02, 2010.
- 255
- 256 Annan, A. P., [2005] Ground-penetrating radar. In *Near surface geophysics*, Butler DK (ed).
257 *Society of exploration geophysicists: Tulsa, Investigations in Geophysics* 13, 357-438.
- 258
- 259 Azaria, A., Zelt, C. A., and Levander, A.: High-resolution seismic mapping at a groundwater
260 contamination site: 3-D travelttime tomography of refraction data. EGS–AGU–EUG joint
261 Assembly, Abstracts from the meeting held in Nice, 2003.
- 262
- 263 Benedetto, A., Tosti, F., Ciampoli, L. B., and D’Amico, F.: An overview of ground-penetrating
264 radar signal processing techniques for road inspections. *Signal Processing*, 132, 201-209, 2017.
- 265
- 266 Cassidy, N. J.: Ground penetrating radar data processing, modelling and analysis. In *Ground
267 penetrating radar: theory and applications*, Jol HM (ed). Elsevier:Amsterdam, 141-176, 2009.
- 268
- 269 Comas X., Slater L. and Reeve A.: Geophysical evidence for peat basin morphology and
270 stratigraphic controls on vegetation observed in a northern peat land. *Journal of Hydrology*, 295,
271 173-184, 2004.
- 272
- 273 Daniels, D.J.: *Ground penetrating radar* (2nd edition). The Institution of Electrical Engineers:
274 London, 2004.
- 275
- 276 Dobecki, T. L.: *Geophysical Exploration at the Giza Plateau, Egypt aTen-Year Odyssey*.
277 *Environmental & Engineering Geophysical Society (EEGS)*. 18th EEGS Symposium on the
278 *Application of Geophysics to Engineering and Environmental Problems*, 2005.
- 279
- 280 El-Arabi, N., Fekri, A., Zaghoul, E. A., Elbeih, S. F., and laake A.: Assessment of
281 Groundwater Movement at Giza Pyramids Plateau Using GIS Techniques. *Journal of Applied
282 Sciences Research*, 9(8), 4711-4722, 2013.
- 283
- 284 Grelle, G. and Guadagno, F. M.: Seismic refraction methodology for groundwater level
285 determination: “Water seismic index”. *Journal of Applied Geophysics* 68, 301–320, 2009.
- 286

287 Griffiths D. H. and King R. F.: Applied geophysics for Engineering and geologists, Pergamon
288 press, Oxford, New York, Toronto, 221p, 1965.
289

290 Harari, Z.: Ground-penetrating radar (GPR) for imaging stratigraphic features and
291 groundwater in sand dunes. *J. Appl. Geophys.*, 36, 43–52, 1996.
292

293 Jol, H. M. and Bristow C. S.: GPR in sediments: advice on data collection, basic processing and
294 interpretation, a good practice guide. In *Ground penetrating radar insediments*, Bristow CS and
295 Jol HM (eds). Geological Society: London, Special Publication 211; 9- 28, 2003.
296

297 Loke, M. H., and Barker, R. D.: Rapid least-squares inversion of apparent resistivity pseudo-
298 sections by a quasi- Newton method. *Geophysical Prospecting*, 44 (1), 131–152, 1996.
299

300 Loke M. H.: Tutorial: 2-D and 3-D electrical imaging surveys. Course Notes, 2012.
301

302 Mahmoud, A. A., and Hamdan, M. A.: On the stratigraphy and lithofacies of the pleistocene
303 sediments at Giza pyramidal area, Cairo, Egypt. *Sedimentology of Egypt*, 10, 145-158, 2002.
304

305 Neal A.: Ground-penetrating radar and its use in sedimentology: principles, problems and
306 progress. *Earth science reviews*, 66, 261-330, 2004.
307

308 Schuster, G. T.: Basics of Exploration Seismology and Tomography. Basics of Traveltime
309 Tomography. Stanford Mathematical Geophysics Summer School Lectures. 1998.
310 (<http://utam.geophys.utah.edu/stanford/node25.html>).
311

312 Sharafeldin, M., Essa, K.S. , Sayl, N. , Youssef, ., Diab, Z. E., and Karlı, H.: Geophysical
313 Investigation Of Ground Water Hazards In Giza Pyramids And Sphinx Using Electrical
314 Resistivity Tomography And Ground Penetrating Radar: A Case Study. Extended Abstract, 9th
315 Congress of the Balkan Geophysical Society, Antalya, Turkey, DOI: 10.3997/2214-
316 4609.201702549, 2017.
317

318 Sheehan, J. R., Doll, W. E., and Mandell, W. A.: An Evaluation of Methods and Available
319 Software for Seismic Refraction Tomography Analysis. *JEEG*, 10 (1), 21–34, 2005.
320

321 Steeples, D. W.: Shallow Seismic Methods. In Y. Rubin, & S. S. Hubbard, *Hydrogeophysics* (pp:
322 215-251). Netherlands: Springer, 2005.
323

324 Stipe, T.: A Hydrogeophysical Investigation of Logan, MT Using Electrical Techniques and
325 Sseismic Refraction Tomography. Degree of Master of Science in Geoscience: Geophysical
326 Engineering Option. Montana Tech., 2015.
327

328 Valenta, J., and Dohnal, J.: 3D seismic travel time surveying – a comparison of the time- term
329 method and tomography (an example from an archaeological site). *Journal of Applied*
330 *Geophysics*, 63, 46-58, 2007.
331

332 Yehia A.: Geological structures of the Giza pyramids plateau. Middle East Res. Center, Ain
333 Shams Univ., Egypt, Sci. Res. Series, 5, 100-120, 1985.

334
335 Zelt, A. C., Azaria, A., and Levander, A.: 3D seismic refraction travel time tomography at a
336 groundwater contamination site. *Geophysics*, 58(9), 1314–1323, 2006.

337
338 Zhang, J., and Toksoz, M.: Nonlinear refraction traveltome tomography. *Geophysics*, 63(5),
339 1726–1737, 1998.

340
341
342
343
344
345
346
347
348
349
350
351
352
353
354
355
356
357
358
359
360
361
362
363
364
365
366
367
368
369
370
371
372
373
374

375

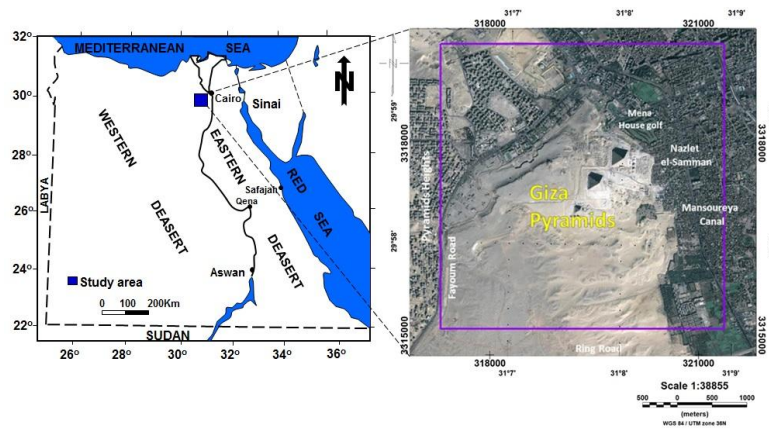


Fig. 1: Location map of the study area of Pyramids Plateau.

376
377
378

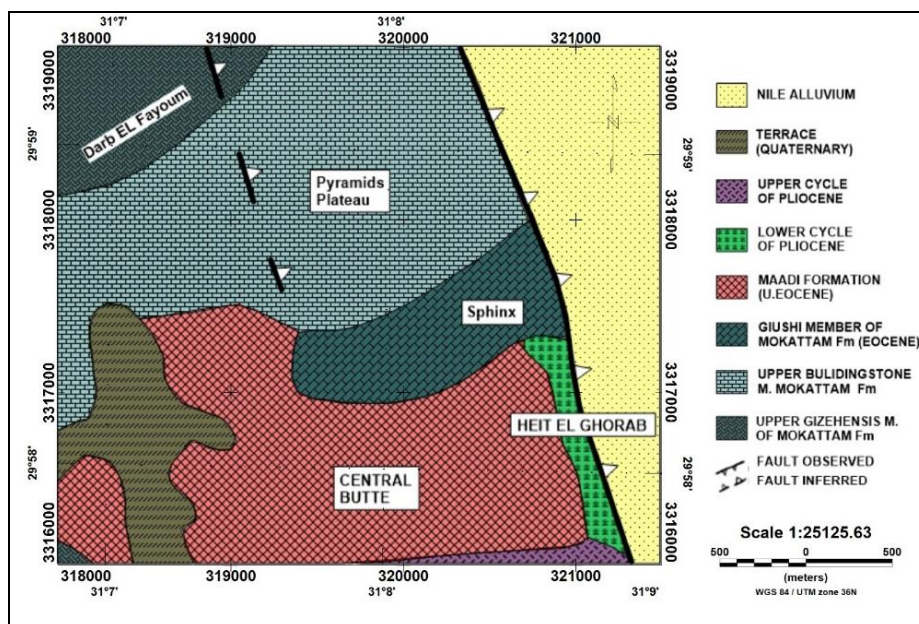


Fig. 2: Geologic map of the Giza Pyramid Plateau, Egypt. (Modified after Yehia, 1985).

379
380
381
382
383
384
385
386
387
388
389
390
391
392
393
394
395
396
397
398
399
400
401
402

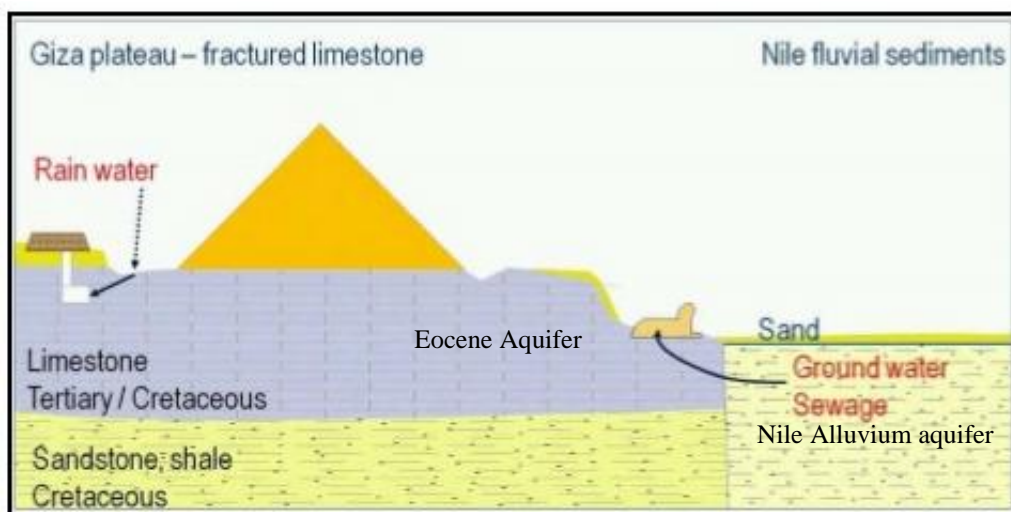
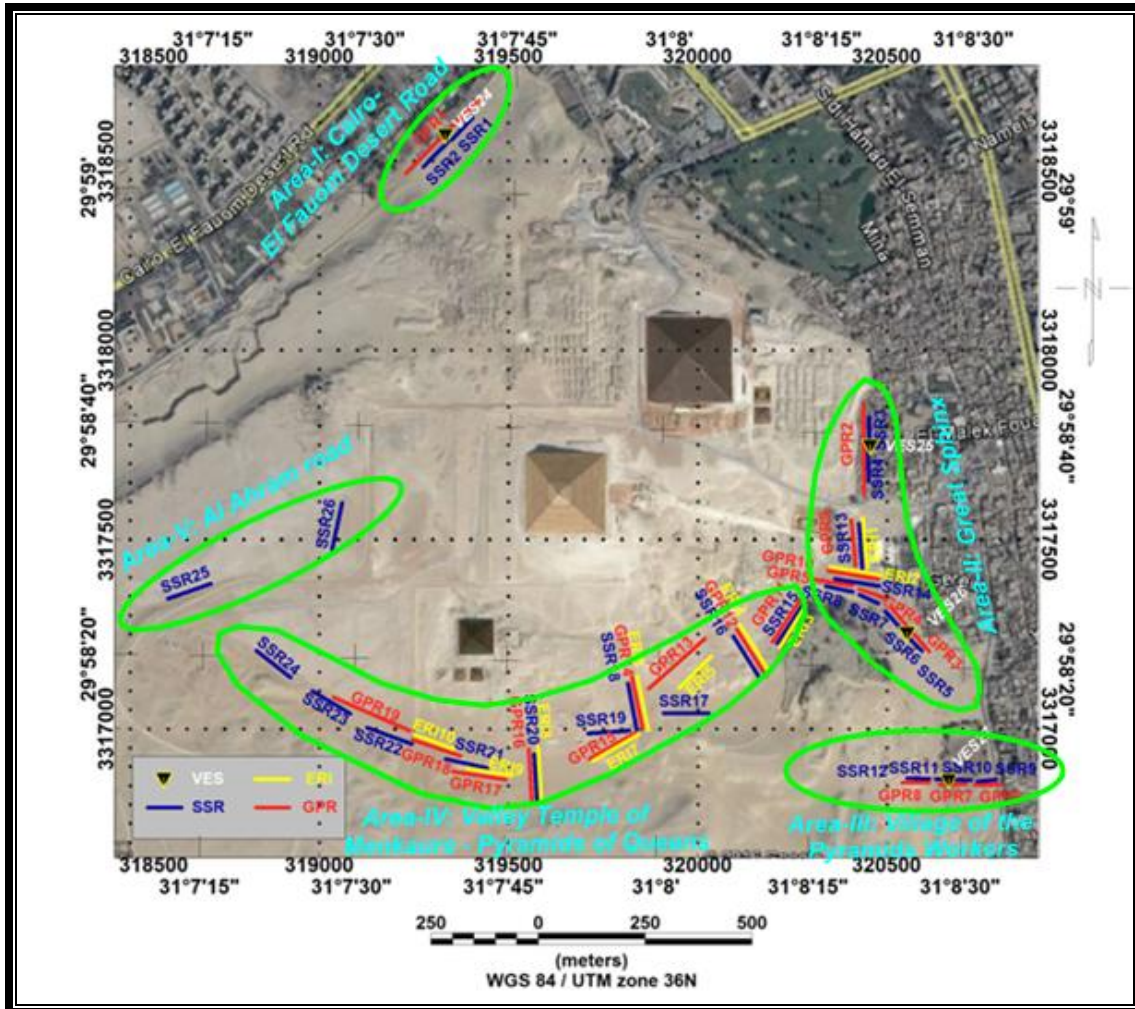


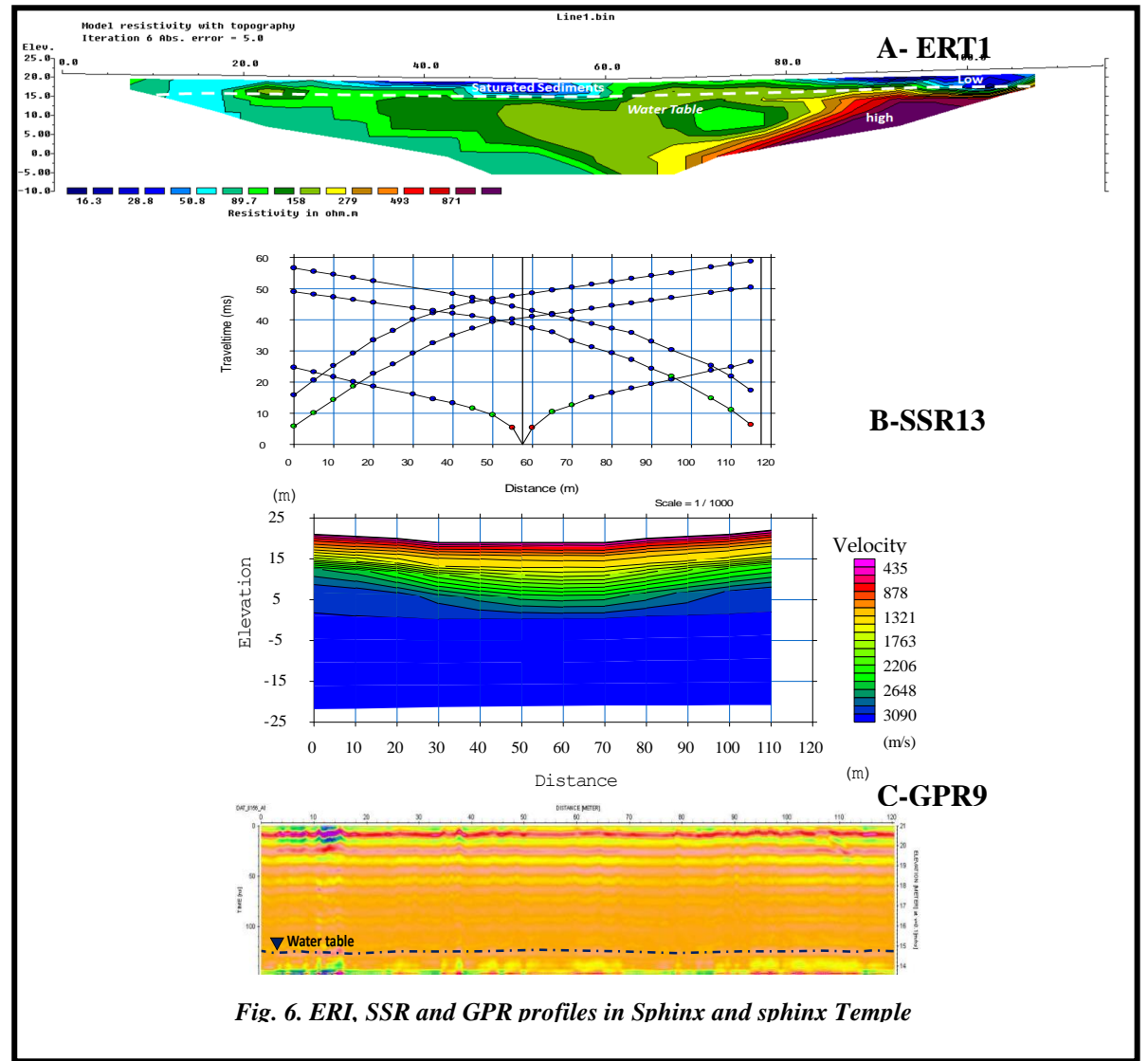
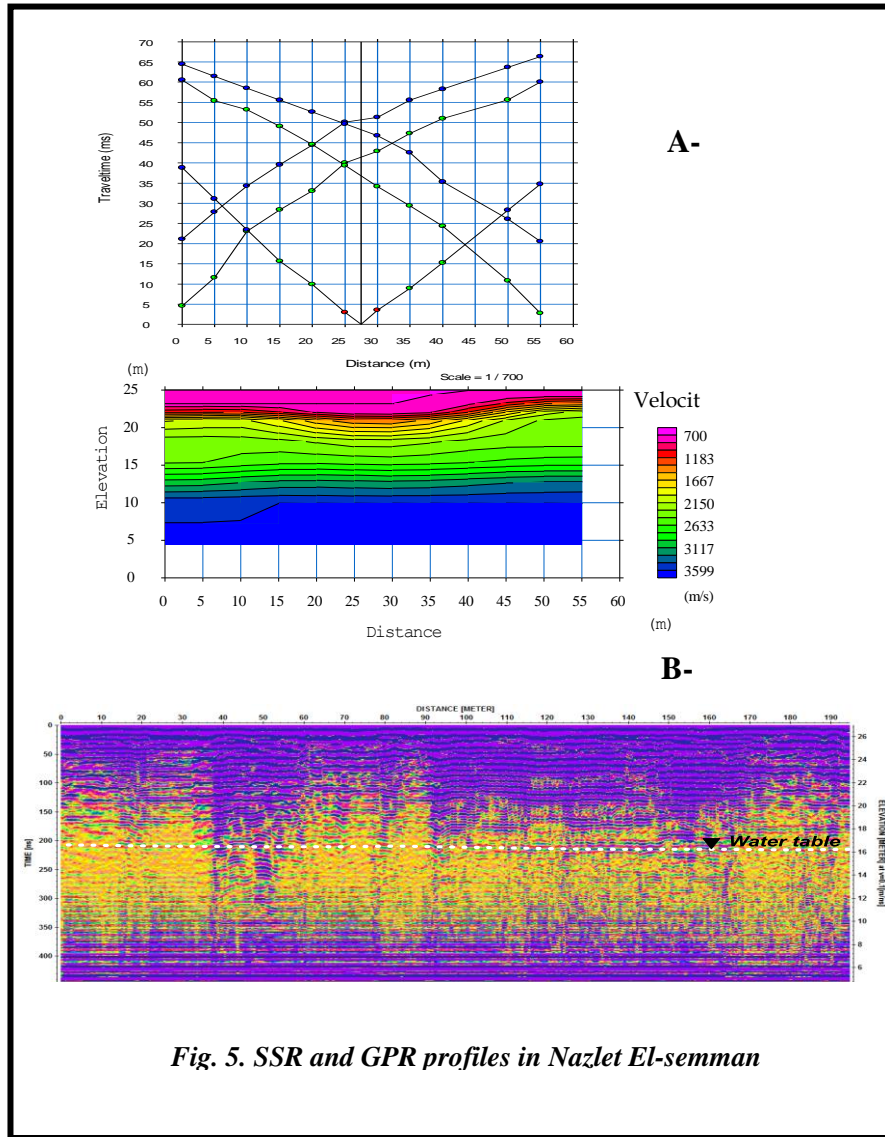
Fig. 3 Ground water aquifers affected the Giza Pyramids Plateau (El-Arabi et al., 2013).

403
404
405
406
407
408



409
410

Fig. 4: locations for the profiles and techniques used along the different parts of the Giza Pyramids plateau.



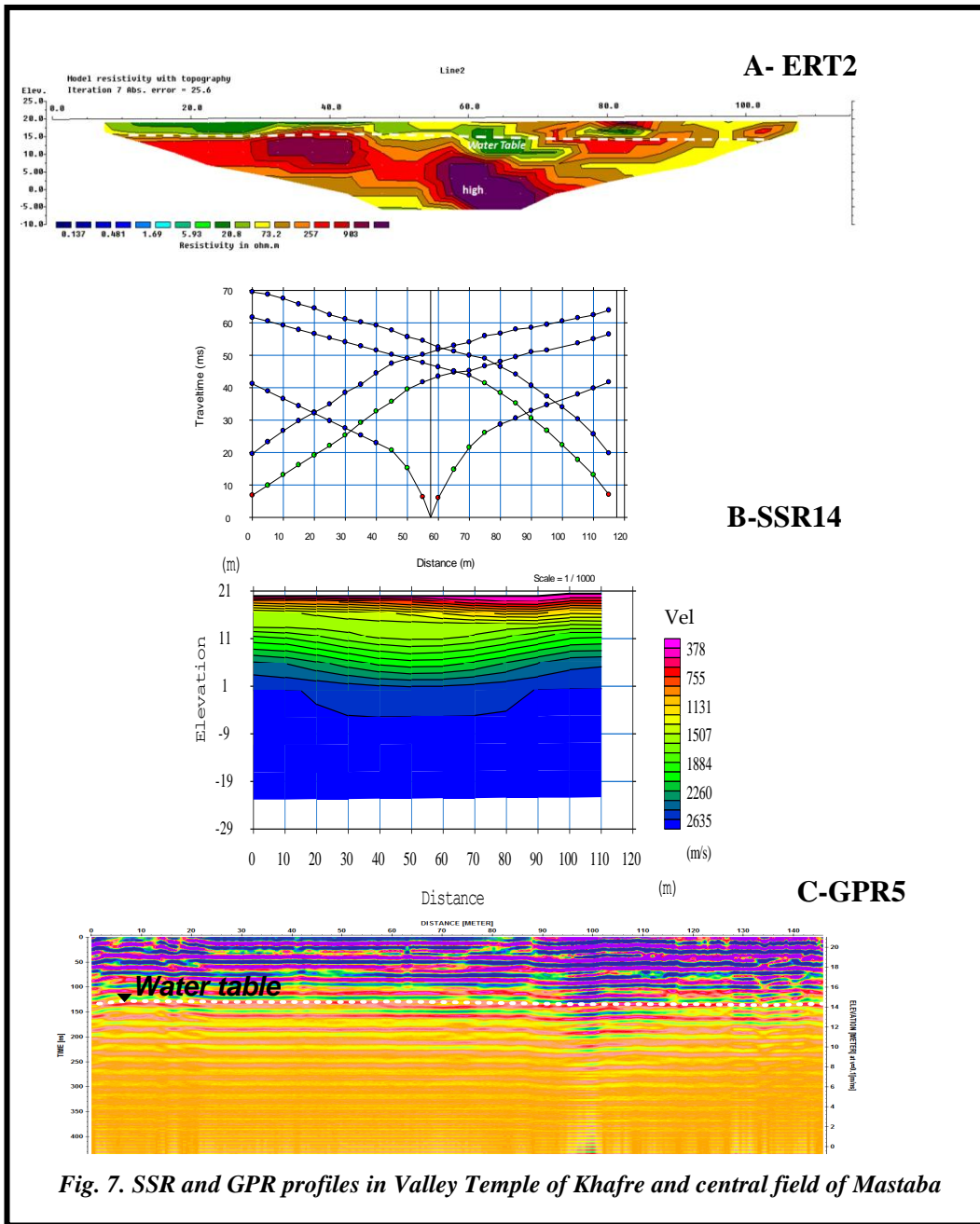


Fig. 7. SSR and GPR profiles in Valley Temple of Khafre and central field of Mastaba

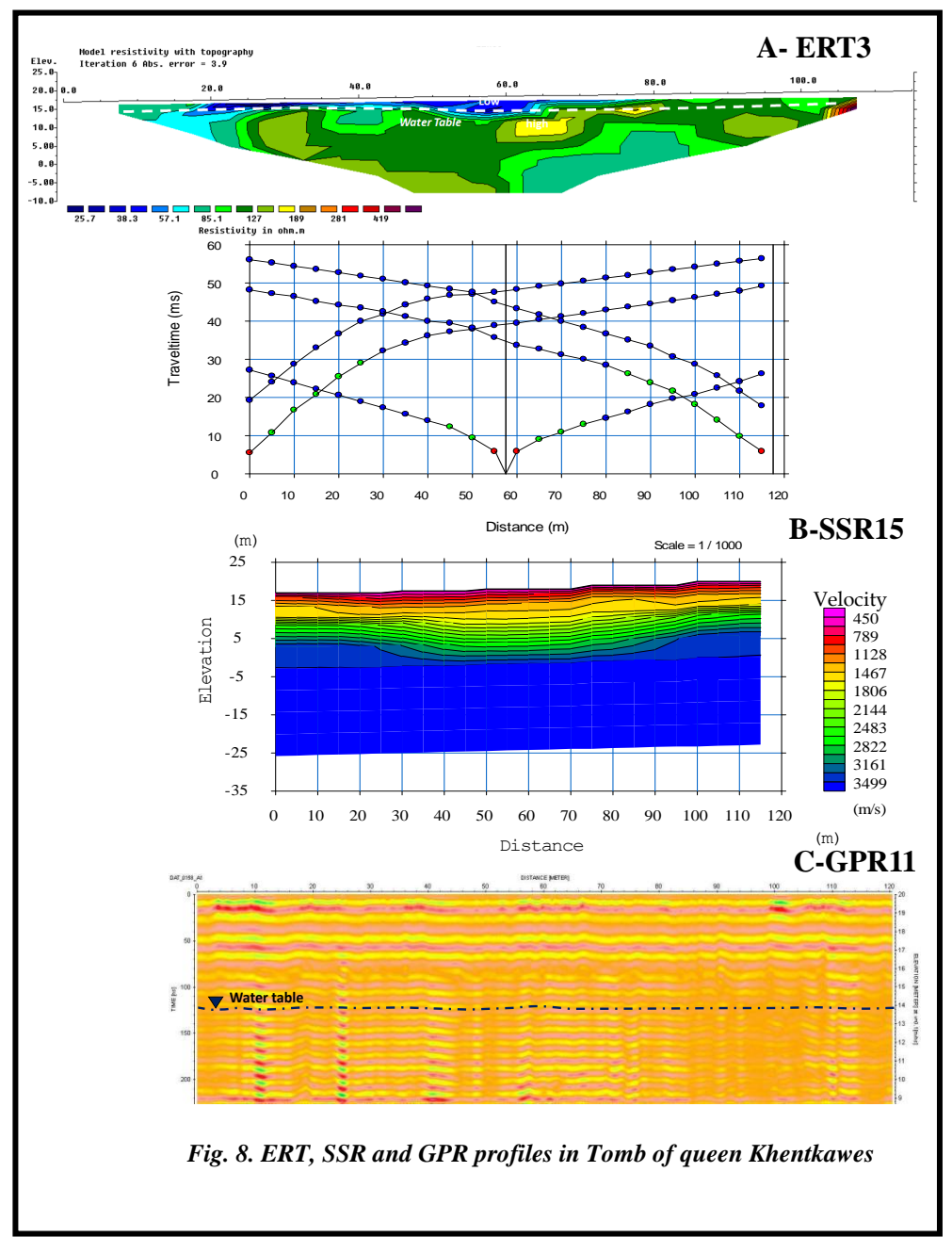


Fig. 8. ERT, SSR and GPR profiles in Tomb of queen Khentkawes

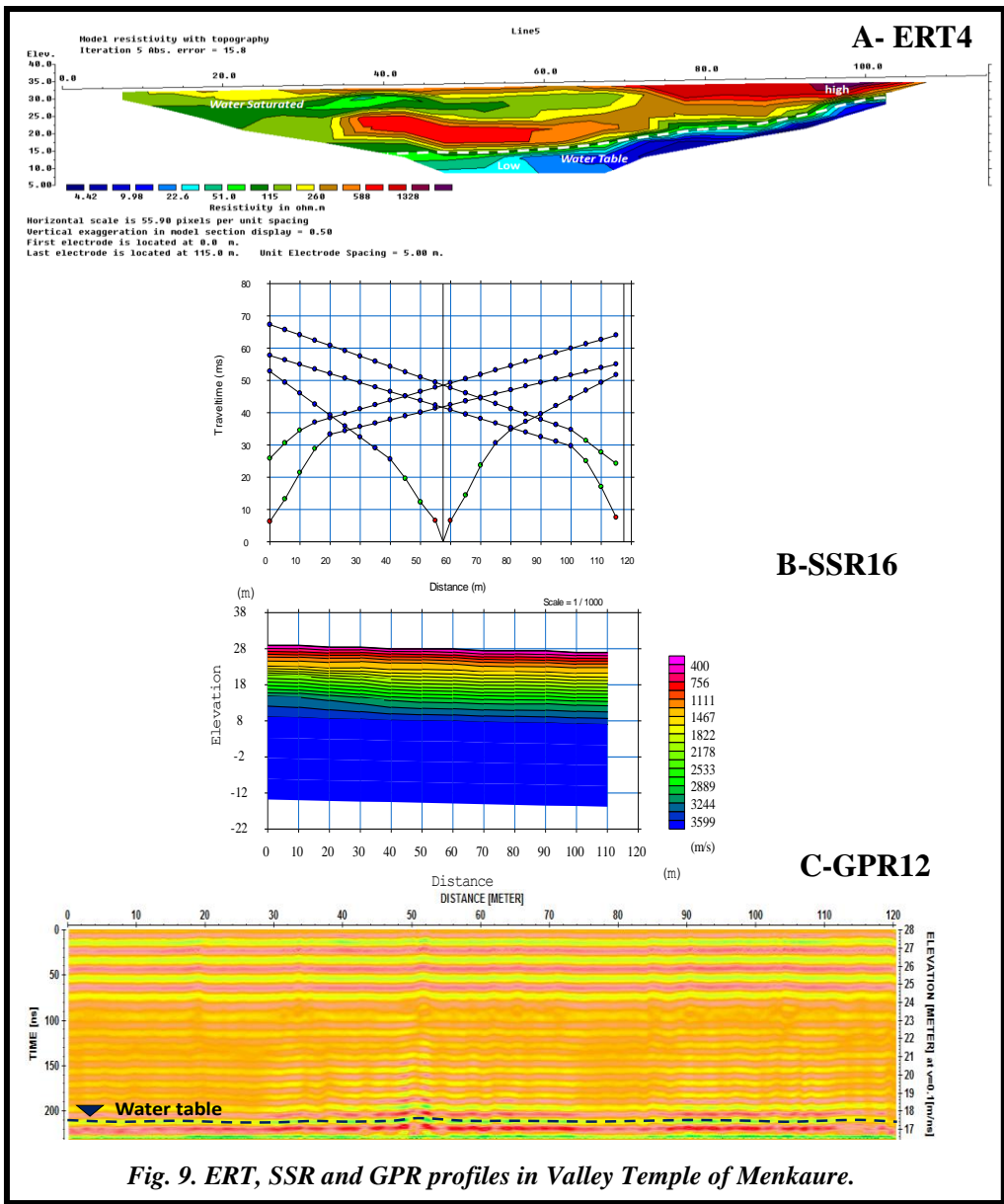


Fig. 9. ERT, SSR and GPR profiles in Valley Temple of Menkaure.

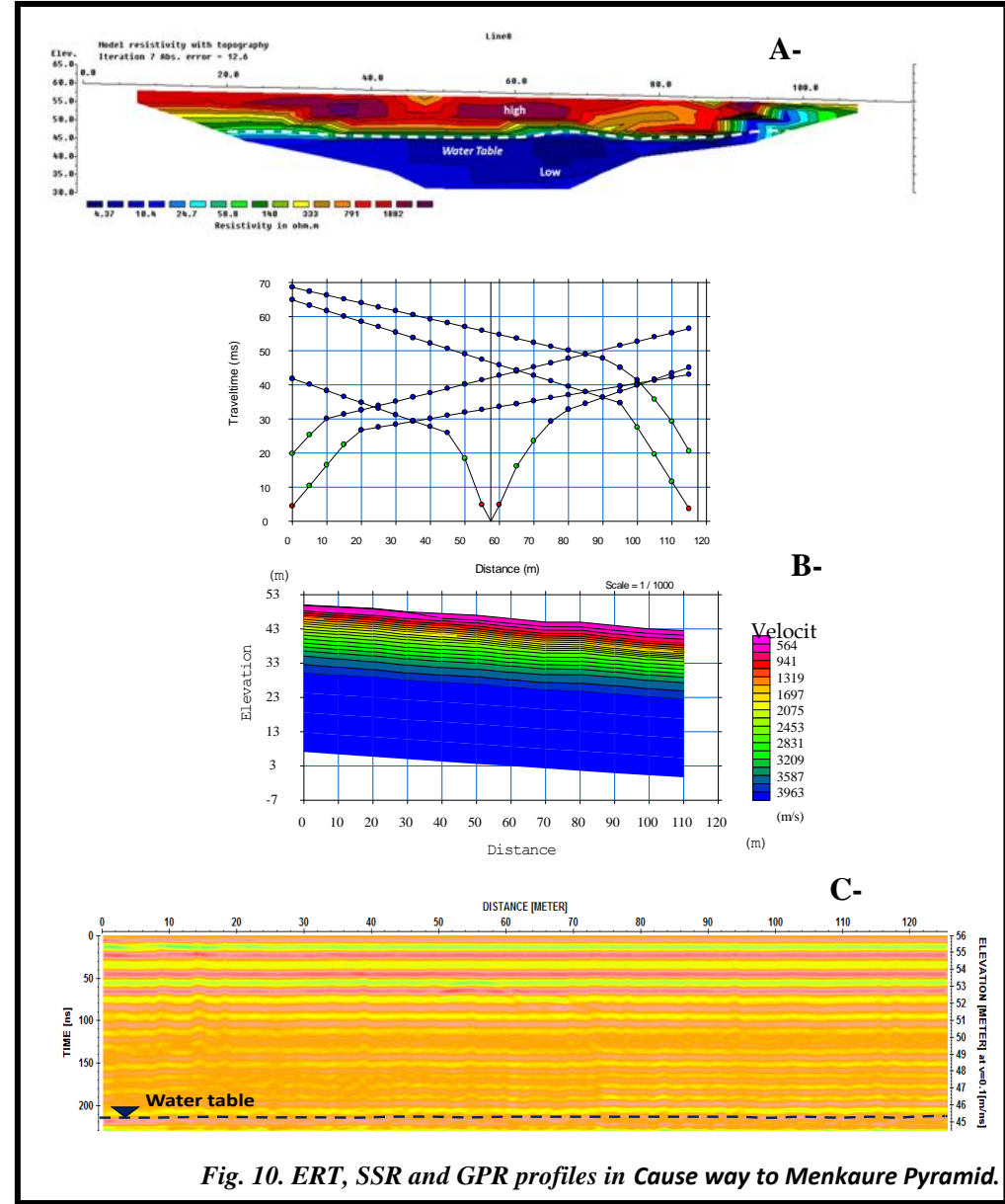
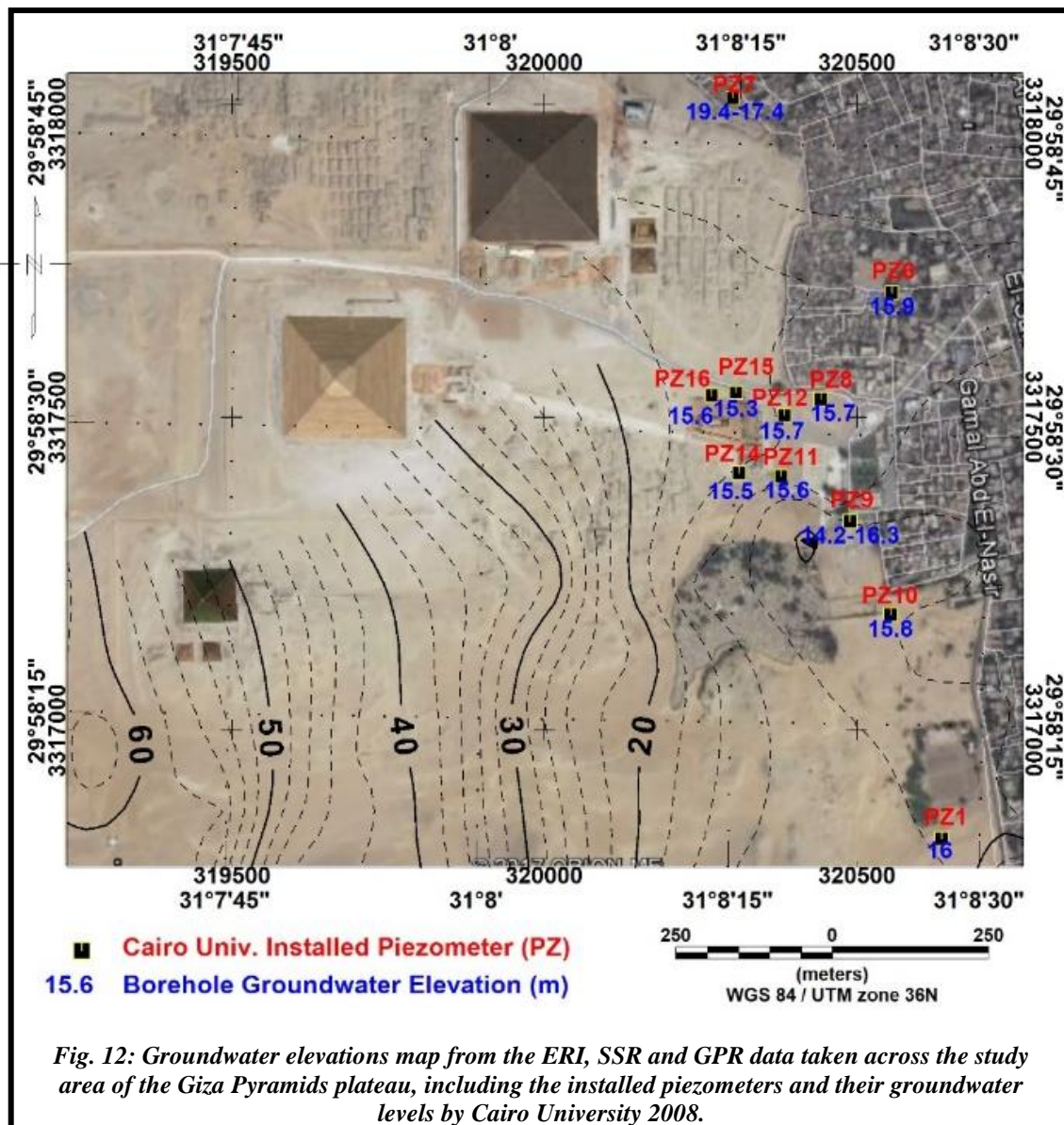
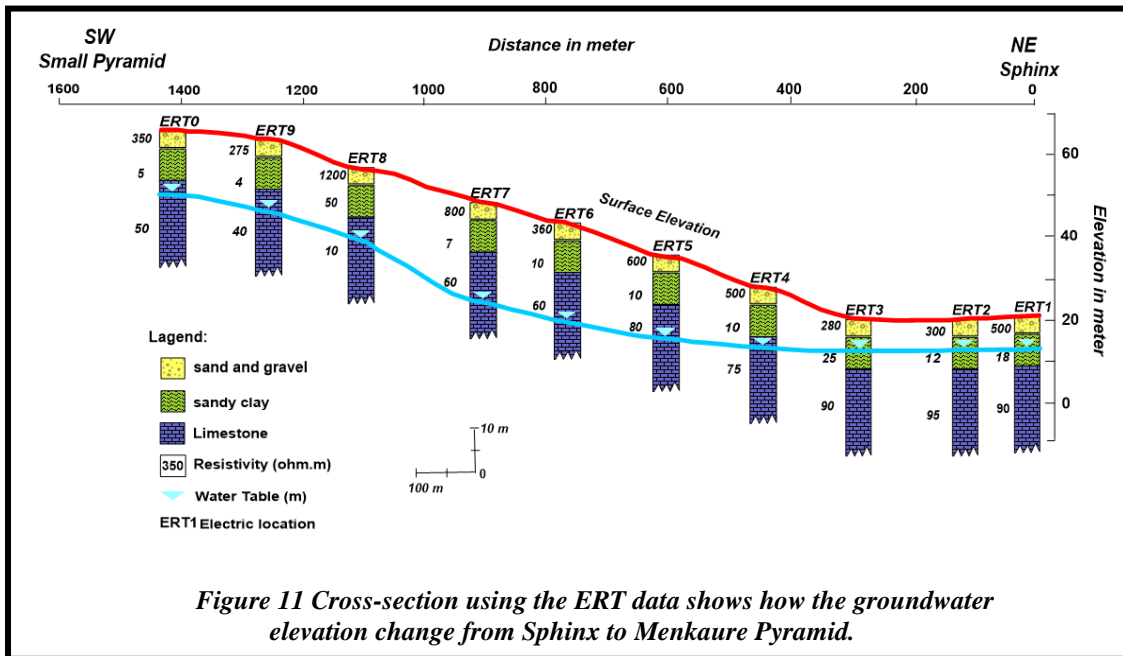


Fig. 10. ERT, SSR and GPR profiles in Cause way to Menkaure Pyramid.



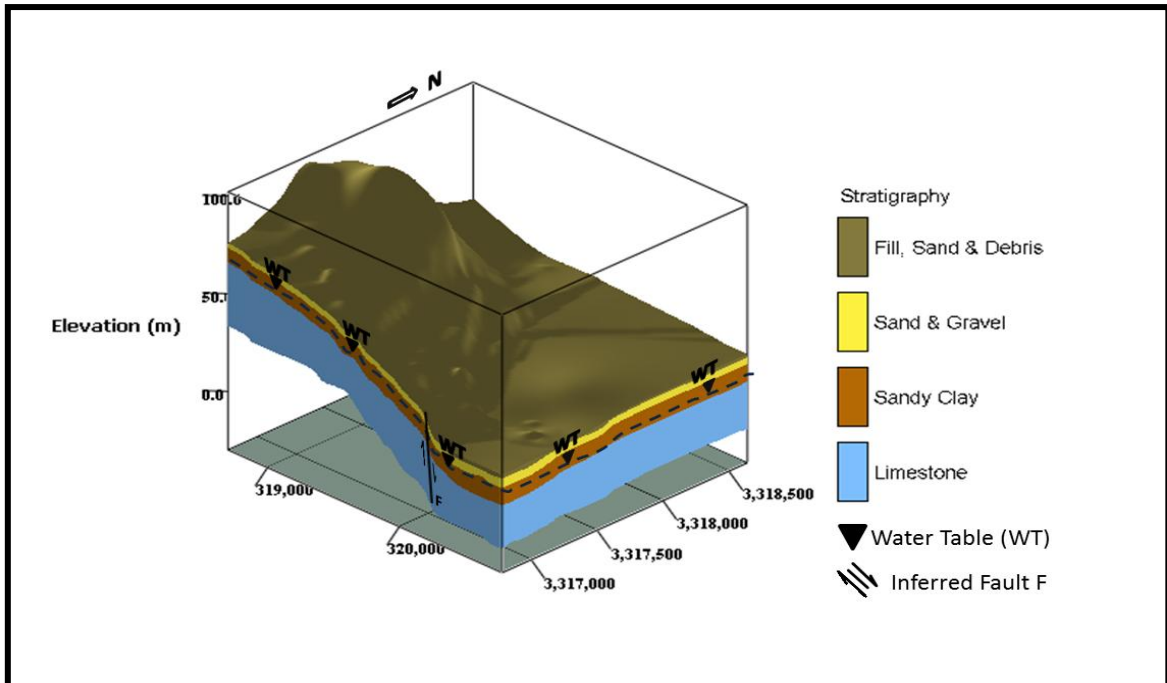


Fig. 13: 3D model of the Giza Pyramids Plateau, illustrating the groundwater table.

Author's response to the Associate Editor comment on the paper entitled "Shallow Geophysical Techniques to Investigate the Groundwater Table at the Giza Pyramids Area, Giza, Egypt" gi-2017-39

Authors: S. M. Sharafeldin, K. S. Essa, M. A. S. Youssef, H. Karsli, and Z. E. Diab, N. Sayil

We would like to thank Prof. Lev Eppelbaum, Associate Editor, for his keen interest, valuable comments on the manuscript, and improvements to this work.

Replies to the comments of the reviewer

Comment #1:-

"Dear authors, I have read your manuscript and I found it is interesting. I have some modifications:

- 1- where the figures of the manuscript, I did not find them.**
- 2- the manuscript needs some moderate language revision".**

Reply:

Thank you. We have corrected, modified and added the missing figures.

Thank you